Lateral development of electron showers measured by silicon microstrip detectors

Y.H. Chang, A.E. Chen, S.R. Hou*, K.T. Huang, C.H. Lin, W.T. Lin
Physics Department, National Central University, Chungli 32054, Taiwan ROC

Abstract

We present a study of lateral shower profiles using granular silicon microstrip detectors for electrons of momenta from 2 to 50 GeV. The absorbers used are lead, copper and tungsten from 0.5 to 4 X_0. The measurements of lateral shower spectra and shower multiplicities are compared to full GEANT simulations.

*Corresponding author. Tel +41 22 767 9358, Fax +41 22 782 8923, e-mail Suen.Hou@cern.ch

1 Introduction

The use of silicon detectors for sampling calorimeters has provided compactness and granularity. Their energy response has high resolution and good linearity. The detector segmentation and sampling scheme rely on a good understanding of the shower development. In this report we present a study of the lateral shower profiles sampled by silicon microstrip detectors for incident electrons of energies from 2 to 50 GeV. The materials used for the absorber are lead, copper and tungsten ranging in thickness from 0.5 to 4 X_0.

Electromagnetic shower development is better understood in longitudinal profiles [1]. Recent studies on lateral shower profiles reported include the SICAPO [2] collaboration using silicon strips of 1 mm pitch and SPACAL [3] using a scintillation fiber calorimeter. A sampling calorimeter has the advantage of detecting the shower incident position by measuring the shower secondaries before the shower maximum, as the shower consists of only a few high momentum particles within a small angular range. A preshower detector using silicon strip detectors is proposed by RD36 [4] for LHC experiments. An earlier study [5] has achieved a spatial resolution of 100 μm for measuring the shower incident position of 50 GeV electrons with an aluminum absorber of 1.4 X_0.

The readout pitch of the silicon microstrip detectors used to sample the shower is 50 μm. The thickness of the silicon wafer is 320 μm, it corresponds to a most probable ionization loss of about 90 keV [6] for a traversing charged particle. The fine-grained pitch and the high detection efficiency of the silicon microstrip detector has provided excellent spatial resolution for the detection of charged particles.

We first describe the experimental setup, including the parameters of the detectors and absorbers. Then we discuss the algorithm for reconstructing the particle's impact position on the silicon wafer by using the ionization charge collected by a cluster of adjacent strips. The beam line configuration has been simulated by GEANT [7] with the cutoff thresholds tuned to data for electrons, photons and δ-ray electrons. There are two layers of silicon wafers positioned behind the absorber. The lateral shower profile of charged particles is measured as the charge weighted cluster distribution. It has a wide halo and a dense shower core. The shower envelope can be parameterized with a double Gaussian distribution [1] which incorporates contributions from the core and halo. The measured shower profiles are compared to GEANT simulations.

The ultimate ability to resolve close tracks from pileup as one reconstructed cluster is limited to a minimum of two readout strips (a double track resolution of about 100 μm in this study). The pileup of shower secondaries is estimated by GEANT simulations. We scale the number of observed clusters according to the GEANT estimations to determine the shower multiplicity of charged particles. We measure the ratio of sail-through events for absorber thickness of 0.5 and 1 X_0 and the most probable shower multiplicities of charged particles for absorber thickness of 2 and 4 X_0.

2 Experimental setup

The investigation was performed at the X3 beam line of the CERN-SPS. Electrons of 2, 4, 10, 25 and 50 GeV were used. Events were triggered by scintillation counters in coincidence with a beam spot dimension of 1×1 cm^2. The beam momentum spread is dominated by the opening width of collimators; wider opening was applied at low beam momentum to gain event rate with $\delta p/p$ between 1% and 8% for particle momenta of 50 and 2 GeV respectively. The beam contamination of MIP particles is less than 3%. MIP events were vetoed by a downstream calorimeter.

The parameters of the six silicon strip detectors used in this study are listed in Table 1. These are single-sided AC-coupled detectors manufactured by ERSO [8]. All of the detectors were operating at full depletion voltage. The signal readout was performed by VA1 circuits [9] with high signal to noise ratio obtained. The data acquisition was an IBM-PC based system interfaced to SRS-SDA modules [10] with 8-bit ADC dynamic range.

The absorbers used were lead, tungsten (90% pure) and copper plates in beam line setup-1, 2 and 3, respectively. Illustrated in Fig. 1 is the configuration of setup-1. Coordinates of detectors in the beam line are listed in Table 1. The absorber plate was positioned in front of Y_5 detector up to 4 X_0. The air gap was 11 mm for lead and copper, 15 mm for tungsten. The combinations of electron beam energy and absorber thickness applied for data taking are listed in Table 2. At higher beam energy (25, 50 GeV) the shower secondaries are much denser in the shower core. It may occur that the particle pileup in a single strip readout exceeds the ADC dynamic range; therefore shower profiles are only studied up to 1 X_0.

3 Event reconstruction

The charge collected by each readout strip is measured in ADC counts (A_i) after the subtraction of its common shift (C_i) and pedestal value (P_i). The common shift is uniform over channels of one VA1 chip. The pedestal value of each channel ($P_i = \langle A_i - C_i \rangle$) is the mean of net ADC of events randomly triggered between beam spills during data taking. The noise level (σ_{Ni}) is the RMS of P_i and we apply the mean ($\sigma_N = \langle \sigma_i \rangle$) on all channels of one detector for the threshold setting.

The ionization charge generated in the silicon wafer by the traversing electron is collected by one or more adjacent strips. These strips form a cluster which is required to have a peak strip charge above $C_p\sigma_N$ with neighboring strips of descending charge to $1\sigma_N$. The total sum is required to be larger than $C_s\sigma_N$. The two thresholds C_p and C_s are chosen to maximize detection efficiency with minimum contamination of random clusters caused by electronic noise.

The noise contamination is examined by searching for clusters in the randomly triggered pedestal events. Hot/dead channels of total about 2% are masked off. The detection inefficiency is the ratio of events with no cluster found in active area. The random noise contamination is eliminated by applying higher cluster thresholds on C_p and C_s; as a consequence the detection inefficiency increases. Illustrated in Fig. 2 are results for Y_5 and Y_6 applying different thresholds. We have chosen $C_p = 5\sigma_N$ and $C_s = 8\sigma_N$ for all detectors in this analysis. The corresponding detection inefficiency

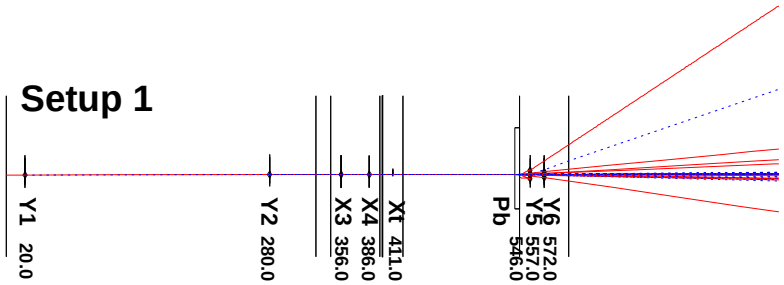

Figure 1: Beam line configuration of setup-1.

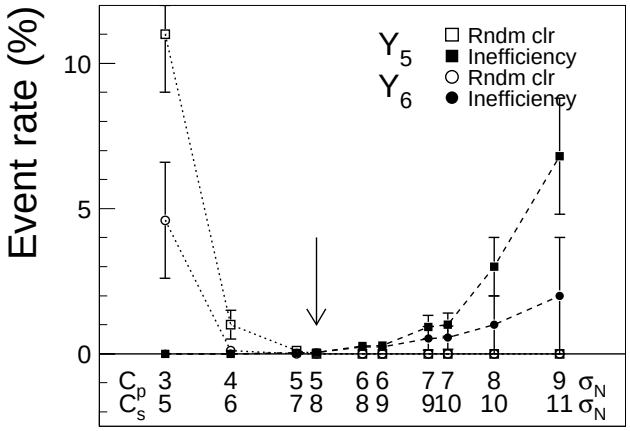

Figure 2: Random noise cluster rate (open marks) and the corresponding detection inefficiency (closed marks) for the cluster selection thresholds C_p and C_s.

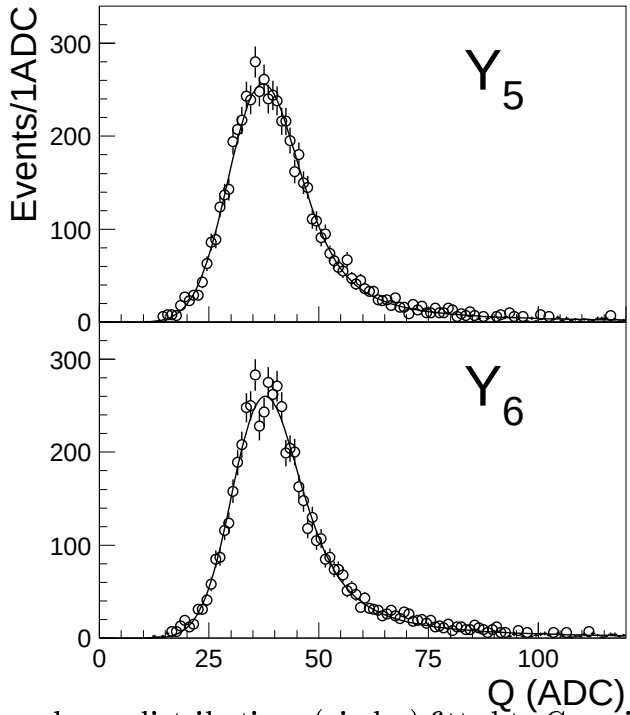

Figure 3: Cluster charge distributions (circles) fitted to Gaussian-convoluted Landau distributions (solid lines).

	Y_1	Y_2	X_3	X_4	X_t	Y_5	Y_6
thickness [μm]	320	320	320	320	320	320	320
active width [mm]	32.0	25.6	64.0	64.0	–	32.0	32.0
strip length [mm]	80	80	40	40	–	80.0	80.0
strip pitch [μm]	25	25	100	100	–	25	25
readout pitch [μm]	50	50	100	100	–	50	50
Setup-1 z position [mm]	20.0	280.0	356.0	386.0	411.0	557.0	572.0
Setup-2 z position [mm]	20.0	280.0	381.0	411.0	496.5	631.5	646.5
Setup-3 z position [mm]	20.0	280.0	355.5	355.5	471.5	606.5	621.5
Noise [ADC]	1.0	1.0	1.5	2.2	–	1.7	1.5
Signal/Noise	26.3	30.0	19.3	12.0	–	20.8	24.0

Table 1: Geometrical parameters of detectors.

E_b [GeV]	Pb [X_0]	W [X_0]	Cu [X_0]
50	0.45, 0.98,	1.0	0.49, 1.05
25	0.45, 0.98,	1.0	0.49, 1.05
10	0.45, 0.98, 1.96, 4.02	1.0, 2.0, 4.0	0.49, 1.05, 2.10
4	0.45, 0.98, 1.96, 4.02	1.0, 2.0, 4.0	0.49, 1.05, 2.10
2	0.45, 0.98, 1.96, 4.02	1.0, 2.0, 4.0	0.49, 1.05, 2.10

Table 2: Combinations of electron beam energy and absorber thickness applied for data taking.

is below 0.1 % with negligible noise contamination.

The single cluster charge distributions of 50 GeV electrons are plotted in Fig. 3 for Y_5 and Y_6. Events are selected for single tracks with all detectors observing only one cluster in the calibration data of 50 GeV electrons. Each charge distribution is fitted to a Gaussian-convoluted Landau distribution [11] (solid line). The most probable value of the fit divided by the noise level σ_N of the corresponding detector is the signal-to-noise ratio; it is also listed in Table 1.

The cluster charge of a cluster containing more than one strip is divided into the sum of left and right strips (Q_r, Q_l) by the cluster center (calculated by center-of-gravity). The η parameter is defined as $\eta = Q_r/(Q_r+Q_l)$. The incident beam particles are randomly distributed between readout strips; however, the η distribution is not uniform due to the nonlinear charge sharing between strips [12]. The cluster position is calculated according to the η value by

$$y = y_0 + p \int_0^\eta f(\eta) \Big/ \int_0^1 f(\eta) \, , \qquad (1)$$

where p is the readout pitch and y_0 the strip offset. The detector alignment is calibrated by unweighted linear track fitting for y_0 and the tilt angle in the wafer plane transverse to the beam.

4 GEANT simulation and precision of shower reference position

Full GEANT simulations were performed for all beam line setups. In the simulations the tracking parameters are calculated automatically (AUTO=1) and the step precision parameter EPSIL is set to 10 μm. A cluster is assigned to a detector when a charged particle traverses the active silicon wafer. The cluster position is the mean of the entrance and exit (or stopping) positions in the wafer. The cluster charge is given by a random sampling on the cluster charge spectrum of the corresponding detector obtained from calibration data of 50 GeV electrons (Fig. 3).

The cluster charge is distributed among the two strips adjacent to the particle incident position. The charge fractions assigned are weighted by center-of-gravity to the cluster position. The electronic noise is added by a random Gaussian smearing of RMS equal to σ_N of the corresponding detector. The cluster is later reconstructed by the same algorithm applied to data with the cluster position calculated by center-of-gravity. Fig. 1 contains an event with typical shower tracks drawn by GEANT in interactive mode.

The spatial resolution of the silicon microstrip detectors is studied by unweighted linear track fitting using calibration data with absorber removed. The residuals of measured cluster positions to the fit contain the deviation due to detector resolution and deflections from multiple scattering. In the simulations the multiple scattering is calculated by Molière theory with the detector resolution simulated by a Gaussian smearing on the reconstructed cluster position. By varying the smearing widths of all detectors till the best agreement is reached on residual widths with data [13], we obtain an average spatial resolution of 5 μm for the Y detectors.

The reference shower center positions on Y_5 and Y_6 are calculated by extrapolating the hits measured by the two upstream reference detectors (Y_1 and Y_2). The extrapolation precision is examined using calibration data for the shower center relative to the reconstructed cluster position. The RMS values obtained are about 20 μm for both detectors as listed in Table 3. The same procedure is performed on the GEANT simulations. The consistency between data and simulations verifies the simulation scheme implemented.

	Setup-1	Setup-2	Setup-3
Y_5 data [μm]	17	22	18
Y_5 MC [μm]	17	21	18
Y_6 data [μm]	17	20	19
Y_6 MC [μm]	18	20	20

Table 3: Extrapolation precision for shower center position.

5 δ-ray and low-multiplicity events

The silicon wafers contain a considerable thickness of material for the production of δ-ray electron and pair-conversions. Each detector has detected a few percent of events containing multiple clusters. Since the readout pitch is 50 μm, the cluster reconstruction can only distinguish adjacent charged tracks separated by minimum

two strips (100 μm). However, the cluster charge is proportional to the number of particles contained (apart from the energy straggling). In the simulations the relevant cutoff thresholds (listed in Table. 4) are chosen for the agreements with calibration data of 50 GeV electrons on the distributions of cluster charge, number of clusters, and separation distance between clusters.

The generation of δ-ray electrons in GEANT [14] is controlled by the parameters LOSS and DRAY (both set to 1). The cutoff threshold DCUTE is chosen to be 200 keV to optimize the agreement with data for 1) event rate containing two clusters, and 2) cluster charge distributions of events containing only one cluster. In Fig. 4 the charge sum of all measured clusters are shown; the constituent events containing one, two and three clusters are shown by lines. The distributions of simulated one cluster events are also plotted by the shaded histograms. As we lower the DCUTE threshold, the simulation gives excessive δ-ray electrons of small deflection angle to the primary electron; the consequent cluster charge spectrum of one cluster events has a tail much higher than data due to the pileup within the 100 μm double track resolution.

In two cluster events, the distributions of the separation distance between the two clusters ($\delta y = |y_1 - y_2|$) are shown in Fig. 5 for data and simulations. The maximum peaks at the edge of double track resolution. The event rates of two detected clusters are higher in data than the GEANT calculations as listed in Table 5. We compare the event rates in 1) the full detection range (maximum δy = 32 mm), and 2) a narrower range with δy <2 mm. The 2 mm separation distance corresponds to an angle 14 (133) mRad subtended at the upstream wafer for Y_5 (Y_6) respectively.

The feasibility of cutoff thresholds chosen for GEANT simulations are further examined using data with 0.45 X_0 lead absorber and various electron energies. Illustrated in Fig. 6 are the distributions of the charge sum of total one and two measured clusters. In the one cluster case the pileup of more than one incident charged particle is seen in the tails. Half of the events in the two cluster case contain more than two particles. The separation distance between clusters of two and three measured clusters are plotted in Fig. 7. The number of entries of simulations are normalized to data in both cases.

CUTGAM	CUTELE	BCUTE	DCUTE	LOSS	DRAY	MULS
10 keV	10 keV	100 keV	200 keV	1	1	2

Table 4: GEANT parameters applied in the simulations.

	full range	$\delta y < 2$mm
Y_5 Data [%]	3.0 ± 0.2	1.5 ± 0.1
Y_5 MC [%]	1.1 ± 0.1	0.63 ± 0.05
Y_6 Data [%]	4.3 ± 0.2	2.1 ± 0.2
Y_6 MC [%]	1.9 ± 0.1	0.87 ± 0.06

Table 5: Event rates that contain two clusters in 1) full detection range and 2) $\delta y < 2$ mm; errors are statistics only.

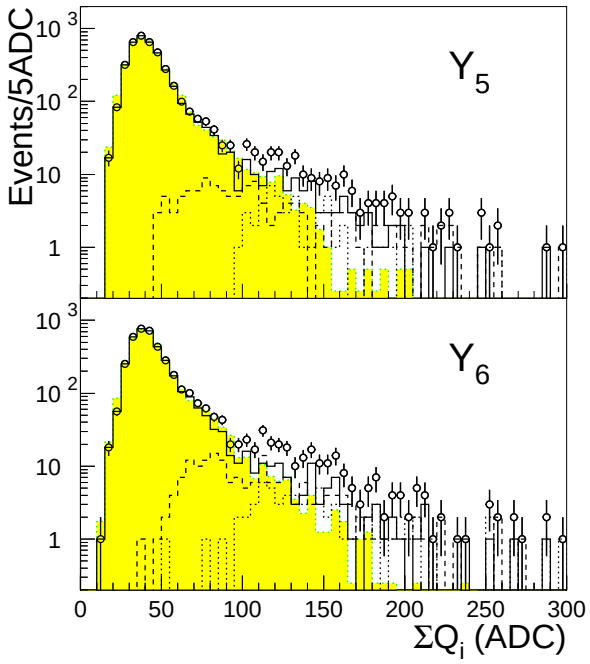

Figure 4: Charge sum of all measured clusters for Y_5 and Y_6 (circles); constituent distributions of events containing one, two and three clusters are shown by the solid, dashed, and dotted lines, respectively. Shaded histograms are the GEANT simulations of events containing only one cluster.

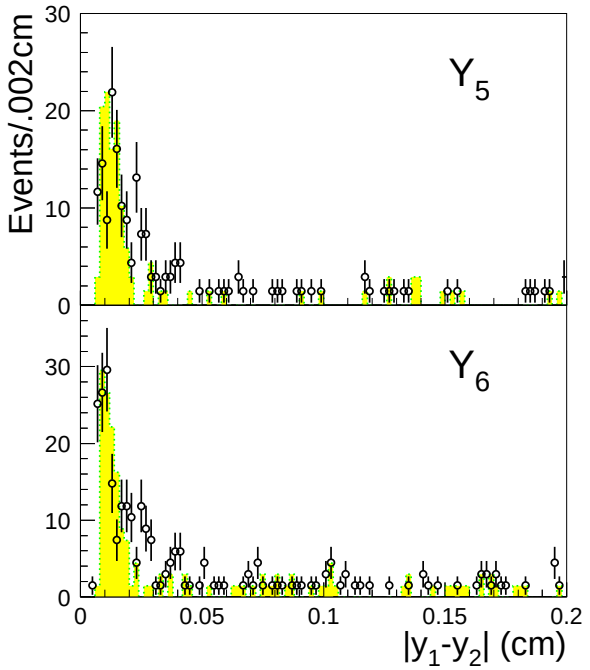

Figure 5: Separation distance between clusters for events contain two clusters (circles); shaded histogram are the GEANT simulations normalized at the peak.

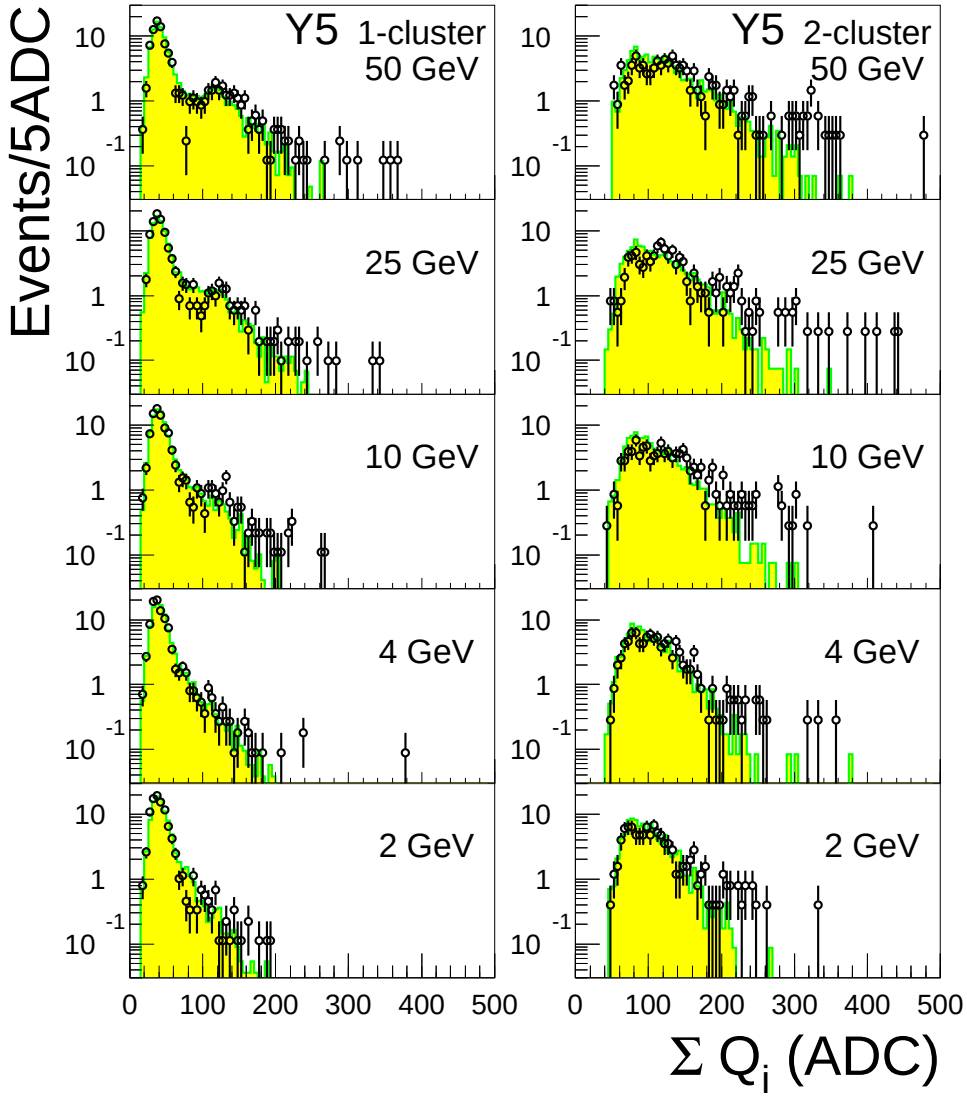

Figure 6: Cluster charge sum of one and two total measured clusters (circles) for Y_5 with 0.45 X_0 lead absorber. Shaded histograms are the GEANT simulations.

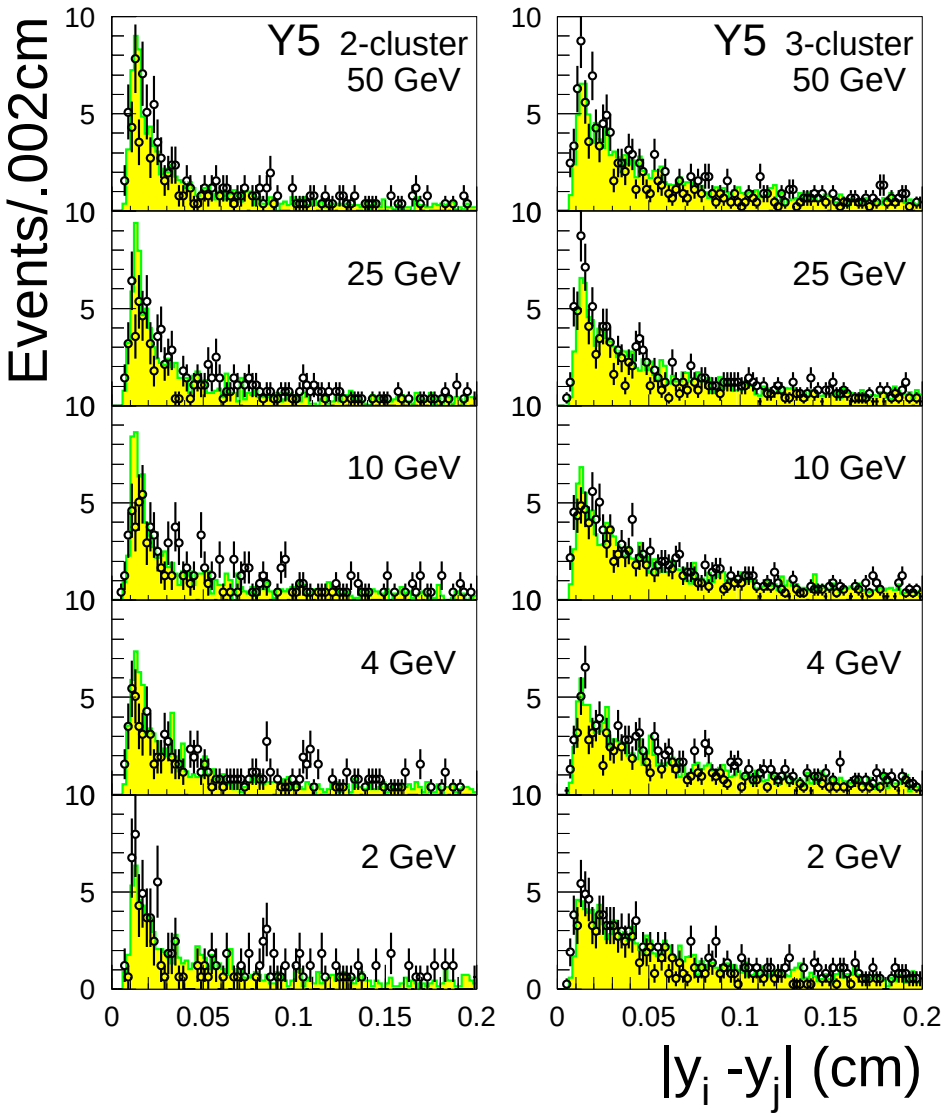

Figure 7: Distance between clusters of total two and three (three entries per event) measured clusters (circles) for Y_5 with 0.45 X_0 lead absorber. Shaded histograms are the GEANT simulations.

6 Lateral shower distributions

Shower events are selected requiring the two upstream detectors to the absorber (Y_1 and Y_2) observe only one cluster. The shower reference center is then calculated by extrapolation. The shower containment is required for the reference shower center in Y_5 and Y_6 to be within a fiducial area of at least 8 mm from the active wafer edges. The shower profiles are studied for absorber thickness up to 4 X_0.

The ionization charge deposit is proportional to the number of particles. The dynamic range of each strip readout has a limit for the pileup of up to five charged particles. The lateral shower spectra shown in Fig. 8 and 9 are the charge weighted cluster distributions detected by Y_5 relative to the shower reference center. The GEANT simulations are shown by the dotted line histograms; solid lines are the generated charged particle densities. The number of events of simulations are normalized to data.

The lateral shower spectrum contains a prominent dense core with wide halo. It is fitted to a double Gaussian distribution of

$$D = C\left(C_{c/h}\exp(\frac{-(y-\bar{y})^2}{\sigma_c^2}) + \exp(\frac{-(y-\bar{y})^2}{\sigma_h^2})\right). \qquad (2)$$

The relevant parameters are σ_c and σ_h representing the shower widths of the core and halo respectively; $C_{c/h}$ is the relative height of them. Each of the lateral distributions in Fig. 8 and 9 is fitted to Eq. 2. Parameters obtained are assembled in Fig. 10 for absorbers of lead, copper and tungsten. The corresponding results of GEANT simulations are plotted in dotted lines of descending (ascending) order to the energy for $\sigma_{c,h}$ ($C_{c/h}$) respectively; solid lines are those for the GEANT-generated charged particle densities.

The shower core is broader for lower electron energy and thicker absorber; at 0.5 X_0 the core RMS is about 200 (20) μm for 2 (50) GeV electrons respectively. The relative height of core to halo drops significantly after 1 X_0. Thus we see that by sampling the lateral shower distributions before 1 X_0 one can achieve a high spatial resolution for the incident position of the electron shower for the energies tested.

The Y_6 detector was positioned 15 mm further downstream to Y_5. The parameters of double Gaussian fits to the spectra of Y_6 are plotted in Fig. 11. Widths obtained are about 20% wider than those of Y_5.

7 Shower multiplicity

The shower multiplicity is measured as the number of clusters scaled by the GEANT estimations for the number of incident charged particles. The fiducial confinement of more than 8 mm to the detector active edge covers $\pm 3\sigma_h$ of the halo distributions for absorber thickness up to 2 X_0 ($\pm 2\sigma_h$ for 4 X_0). It corresponds to a shower containment above 95%. In Fig. 12 the Y_5 measured number of clusters are shown for different electron energies; shaded histograms are the GEANT estimations and the solid lines are the simulated number of incident charged particles in the active wafer.

The fraction of one cluster events in each distribution in Fig. 12 is extracted to measure the ratio of sail-through (one particle) events. The event rate of single

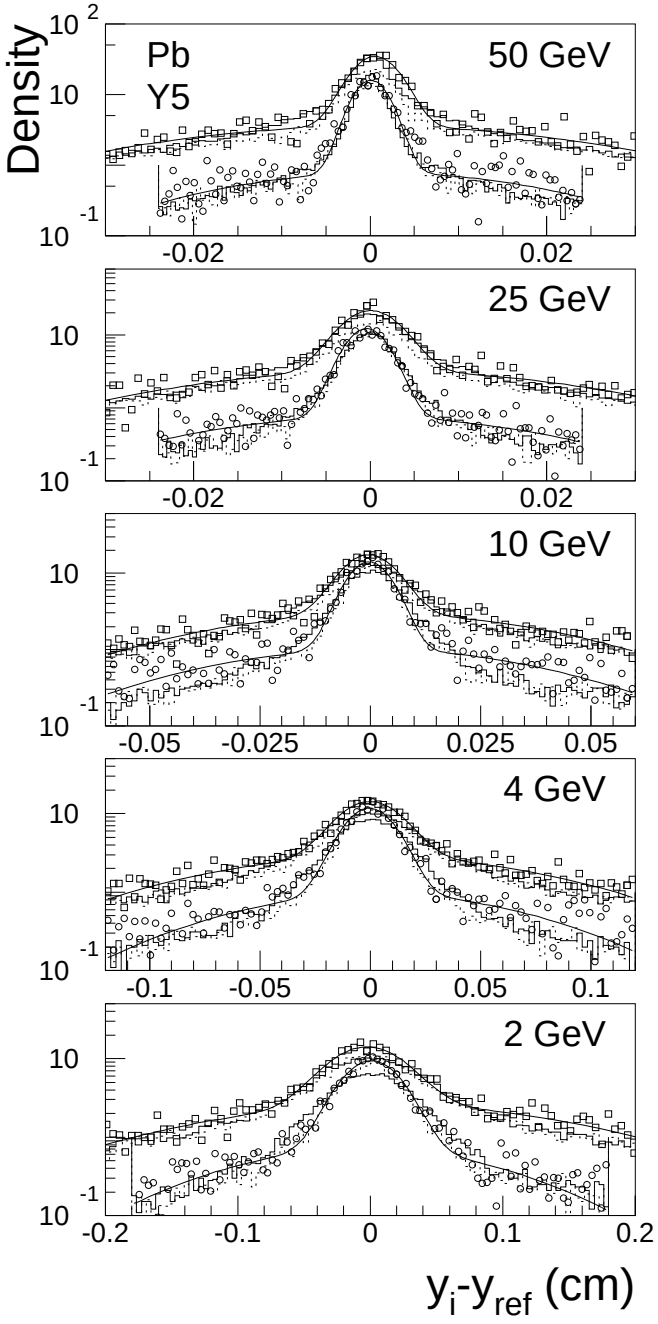

Figure 8: Lateral shower spectra measured by Y_5 for lead absorber of 0.45 (circles) and 0.98 X_0 (squares). Histograms are the GEANT simulations for lateral shower spectra (dotted lines) and generated charged particles densities (solid lines). The curves are the double Gaussian fits to data.

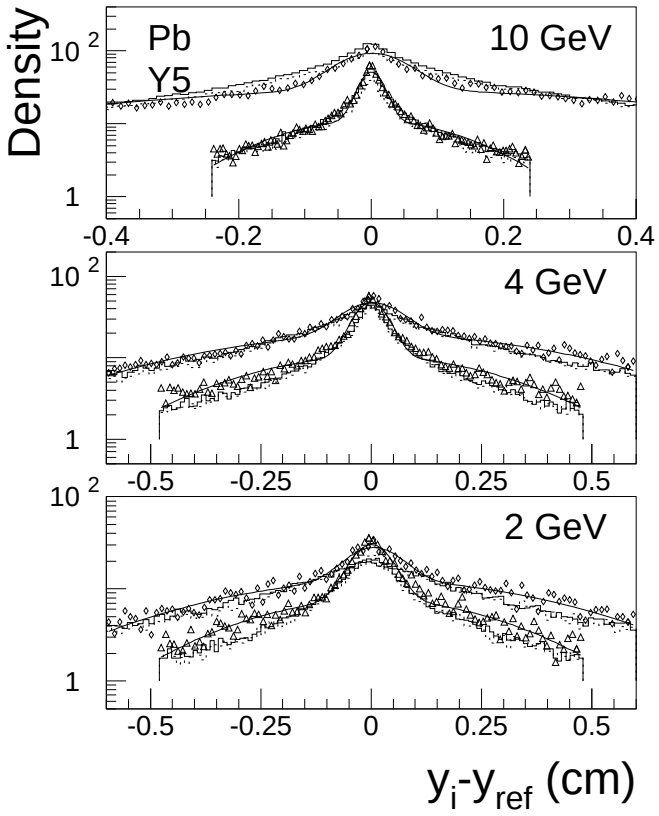

Figure 9: Lateral shower spectra measured by Y_5 for lead absorber of 1.96 X_0 (triangles) and 4.02 X_0 (diamonds). Histograms are the GEANT simulations for lateral shower spectra (dotted lines) and generated charged particles densities (solid lines). The curves are the double Gaussian fits to data.

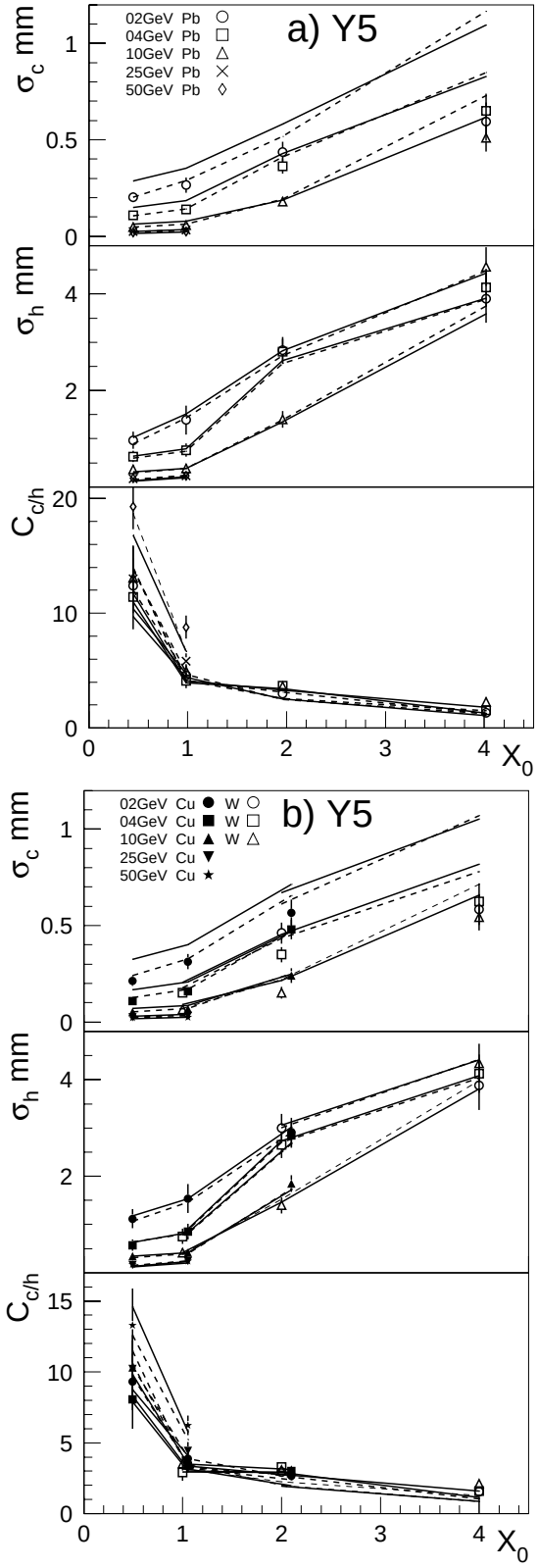

Figure 10: Parameters of double Gaussian fits to the lateral shower profiles for Y_5 measurements (points) and GEANT simulations (dotted lines). Solid lines are those fitted to the GEANT-generated charged particle densities.

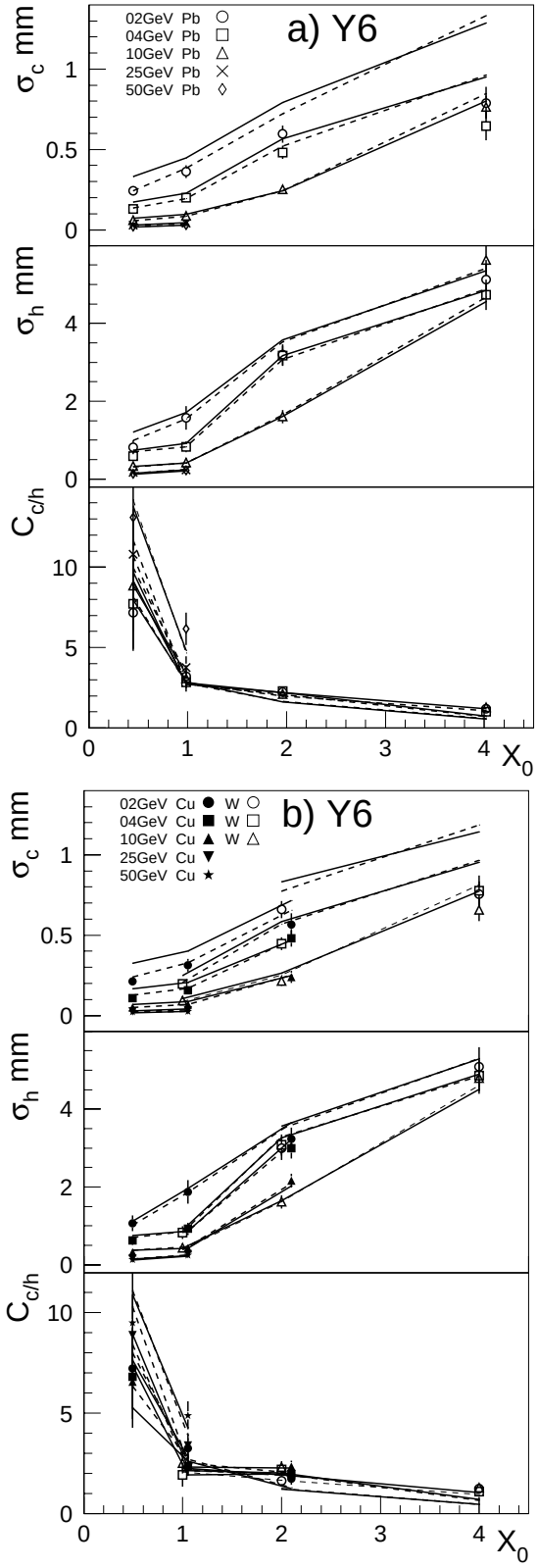

Figure 11: Parameters of double Gaussian fits to the lateral shower profiles for Y_6 measurements (points) and GEANT simulations (dotted lines). Solid lines are those fitted to the GEANT-generated charged particle densities.

cluster contains sail-through and pileup of multiple particles. The pileup rate is estimated by GEANT. It is the ratio of the simulated number of single clusters to the number of single incident particles. The pileup contribution in the single cluster events is scaled off. The sail-through rate measured by Y_5 is illustrated in Fig. 13. The lines are the GEANT calculations for the event rate of single incident particles. The sail-through rates measured by Y_6 are slightly lower. The differences to Y_5 (δR_1) are also shown.

The average number of clusters measured increases significantly for absorber plates of 2 and 4 X_0. Shown in Fig. 14 are the distributions of number of clusters measured by Y_5 (dots). The GEANT predictions for incident charged particles (solid line) and the number of clusters (shaded histogram) are also shown for comparison. Each distribution is fitted to an asymmetric Gaussian function of

$$D = C\exp(\frac{-(N-N_{mp})^2}{\sigma^2}); \qquad \sigma = \sigma_a \text{ if } N > N_{mp}$$
$$\sigma = \sigma_b \text{ if } N < N_{mp} \tag{3}$$

where σ_a, σ_b are the width applied for the regions above and below the most probable value (N_{mp}) respectively. The curves illustrated in Fig. 14 are the fits to data.

In each beam line configuration, the most probable values obtained from the two GEANT distributions give a correction factor to convert the measured number of clusters to the number of incident charged particles. The scaled N_{mp} values of data plotted in Fig. 15 (points) represents the measured number of incident charged particles. The lines are the N_{mp} obtained from the GEANT simulated number of incident charged particles.

8 Conclusion

The silicon microstrip detectors employed in this study provided granularity and high detection efficiency for the measurement of lateral shower profiles of charged secondary particles. The lateral shower spectrum has a dense core with a wide halo that is fitted to a double Gaussian distribution. The shower envelope is parameterized by the three fitting parameters. The shower multiplicities of charged particles are also measured. We have measured the sail-through event rate for absorber thickness of 0.5 and 1 X_0 and the most probable value of the number of charged particles for absorber thickness of 2 and 4 X_0.

The GEANT simulations have good consistency in lateral shower spectra and shower envelope. However, with the steering parameters determined in this study, lower shower multiplicities are simulated particularly for thin absorber and low incident electron energy.

Acknowledgements

We are grateful to the CERN SPS staff for the excellent beam quality and technical assistance. We thank R. Kellogg and D. Strom for providing us the tungsten plates. This study was partially supported by Taiwan National Science Council (NSC85-2112-M-008-024) and Tsu Yuan-Chi memorial foundation.

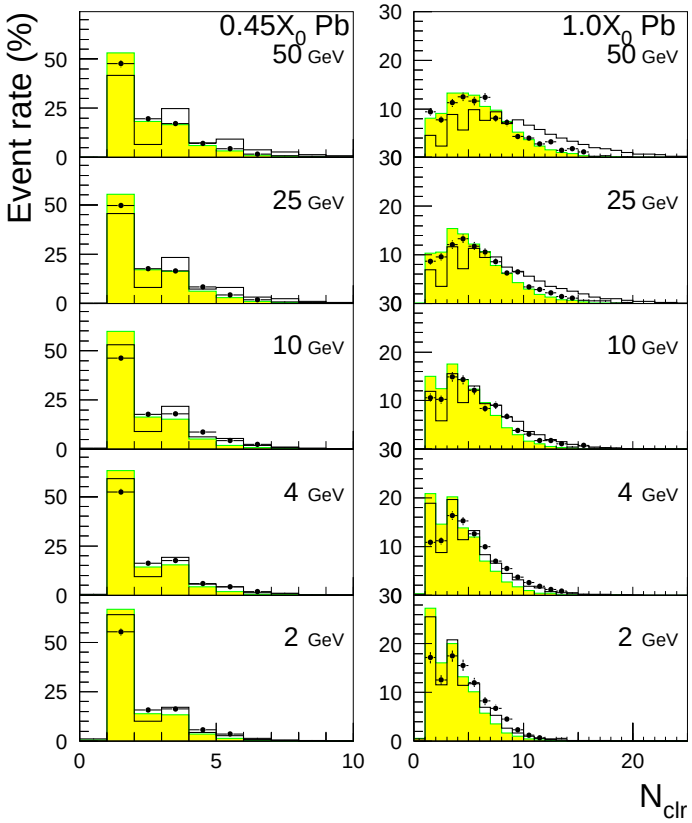

Figure 12: Number of clusters measured by Y_5 for 0.45 X_0 and 1 X_0 lead absorber (dots); histograms are GEANT simulations of number of incident charged particles (solid lines) and reconstructed clusters (shaded).

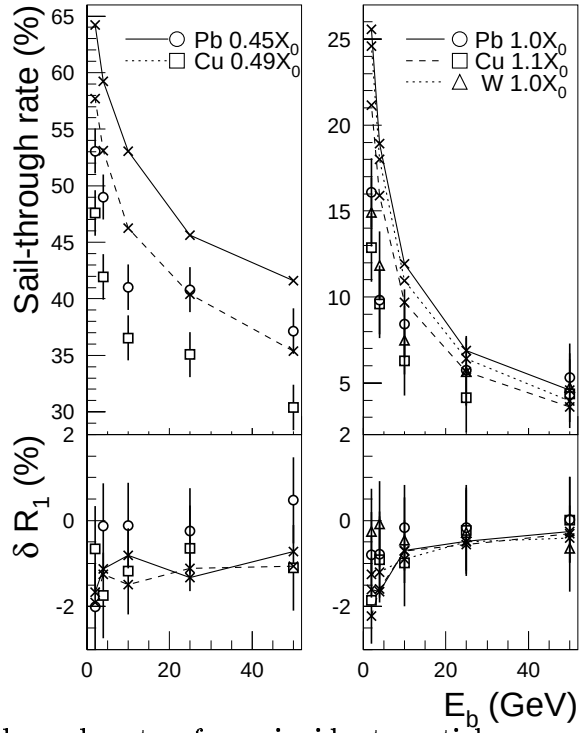

Figure 13: Sail-through rate of one incident particles measured by Y_5; δR_1 is the difference of Y_6 to Y_5. The lines are the GEANT predictions.

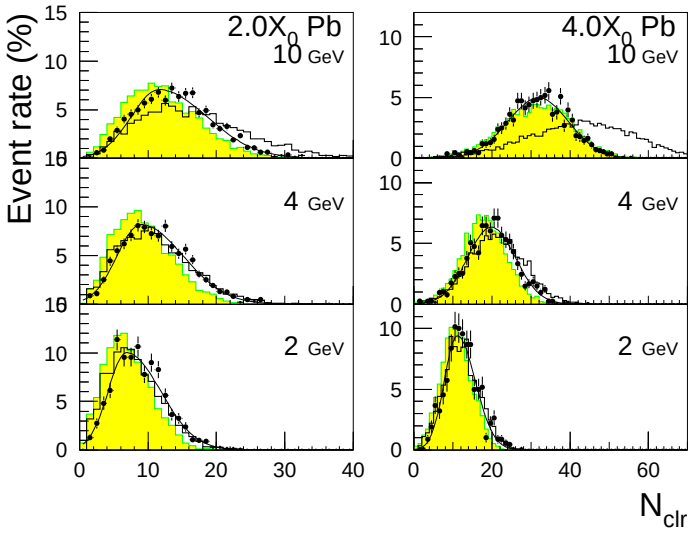

Figure 14: Number of clusters measured by Y_5 for 2 and 4 X_0 lead absorber (dots); histograms are GEANT calculations of number of incident charged particles (solid lines) and reconstructed clusters (shaded). The curves are the asymmetric Gaussian fits to the data.

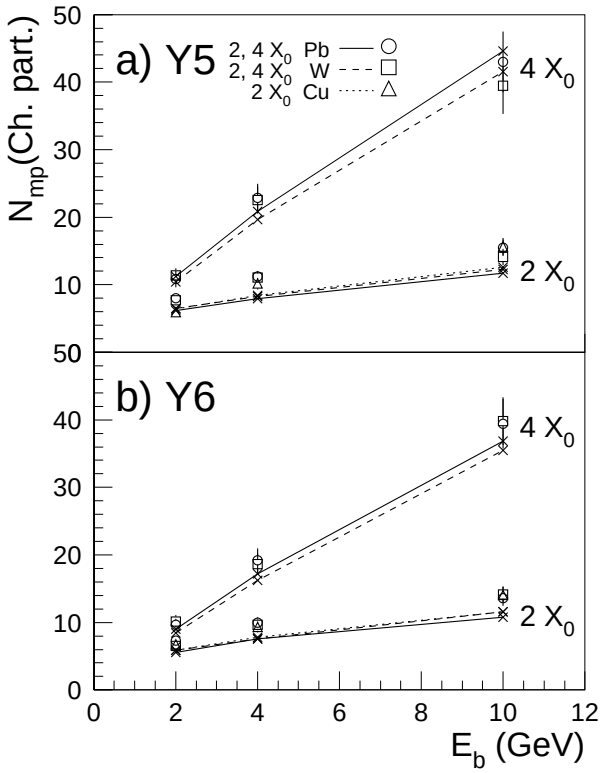

Figure 15: The most probable number of incident charged particles (points); lines are those of GEANT predictions.

References

[1] Review of Particle Physics, Phys. Rev. D 54 (1996) 136, and references therein.

[2] E. Borchi et al. (SICAPO collab.), Nucl. Phys. B Proc. Supp. 23A (1991) 467; G. Ferri et al., Nucl Instr. Meth. A273 (1988) 123; F. Lemeilleur et al., IEEE Trans. Nucl. Sci. NS-34 (1987) 538.

[3] D. Acosta et al. (SPACAL collab.), Nucl. Instr. Meth. A316 (1992) 184.

[4] P. Aspell et al. (RD36 Collab.), Nucl. Instr. Meth. A376 (1996) 17.

[5] Y.H. Chang et al., Nucl. Instr. Meth. A374 (1996) 157.

[6] H. Bichsel, Rev. Mod. Phys. 60 (1988) 663; J.F. Bak et al., Nucl. Phys. B288 (1987) 681.

[7] GEANT Version 3.21 (March 1994); R. Brun et al., CERN DD/EE/84-1 (September 1987), CERN Program Library Long Writeup W5013 (March 1994).

[8] W.C. Tsay et al., Nucl. Instr. and Meth. A351 (1994) 463.

[9] O. Toker et al., Nucl. Instr. and Meth. A340 (1994) 572.

[10] F.A. Kirsten and C. Haber, IEEE Trans. Nucl. Sci. NS-37 (1990) 288.

[11] S. Hancock et al., Phys. Rev. A 28 (1983) 615 and references therein; T. Antičić et al., Nucl. Instr. and Meth. A374 (1996) 309.

[12] E. Belau et al, Nucl. Instr. and Meth. 214 (1983) 253.

[13] Y.H. Chang et al., Nucl. Instr. and Meth. A363 (1995) 538.

[14] L. Urbán, GEANT 3.16 PHYS210 (revised Dec. 1993), CERN Program Library Long Writeup W5013 (March 1994).